Am J Cancer Res 2023;13(11):5236-5253
www.ajcr.us /ISSN:2156-6976/ajcr0152086

Original Article

Risk model-guided identification of MTDH expression as a marker for ferroptosis induction therapy in head and neck squamous cell carcinoma

Xueying Wang[1,2,3*], Yuzhang Gao[1,2,3*], Rui Miao[1,2,3], Lisha Li[4], Abiyasi Nanding[5], Yong Liu[1,2,3,6], Xin Zhang[1,2,3,6]

[1]Department of Otolaryngology Head and Neck Surgery, Xiangya Hospital, Central South University, No. 87 Xiangya Road, Changsha 410008, Hunan, The People's Republic of China; [2]Otolaryngology Major Disease Research Key Laboratory of Hunan Province, No. 87 Xiangya Road, Changsha 410008, Hunan, The People's Republic of China; [3]Clinical Research Center for Laryngopharyngeal and Voice Disorders in Hunan Province, No. 87 Xiangya Road, Changsha 410008, Hunan, The People's Republic of China; [4]Cancer Center, Union Hospital, Tongji Medical College, Huazhong University of Science and Technology, Wuhan 430022, Hubei, The People's Republic of China; [5]Department of Pathology, Harbin Medical University Cancer Hospital, Harbin 150081, Heilongjiang, The People's Republic of China; [6]National Clinical Research Center for Geriatric Disorders (Xiangya Hospital), Changsha 410008, Hunan, The People's Republic of China. [*]Equal contributors.

Received July 7, 2023; Accepted September 24, 2023; Epub November 15, 2023; Published November 30, 2023

Abstract: Head and neck squamous cell carcinoma (HNSCC) are a prevalent malignancy with high mortality and morbidity rates. Therefore, in this study, we aimed to develop a novel risk score model by using a DNA methylation signature associated with ferroptosis to enhance the prognosis prediction of HNSCC. The transcriptome, methylome, and clinical data of HNSCC patients were collected from The Cancer Genome Atlas (TCGA) database. Additionally, data from a methylation dataset in the Gene Expression Omnibus (GEO) database were used for validation. The ferroptosis score (FS) in each patient was calculated using the transcriptome data, and the single-sample gene set enrichment analysis (ssGSEA) was performed to assess ferroptosis activity. Furthermore, a series of biochemical experiments including CCK8, colony formation, wound healing, and ROS detection were carried out to evaluate the influence of MTDH on the malignancy of HNSCC. Our results revealed that the FS was associated with patient prognosis, as the patients with high FS had a poor prognosis. The receiver operating characteristic (ROC) curve established based on the ferroptosis-associated DNA methylation signature, demonstrated the excellent predictive power of FS for the 1-, 3-, and 5-year survival of HNSCC. Importantly, this predictive model was successfully validated in the GEO dataset. The nomogram also demonstrated excellent accuracy and reliability, as determined by the calibration curves and the decision curve analysis (DCA) plot. Interestingly, the risk score model was found to be correlated with immune cell infiltration and immunotherapy-related biomarkers, suggesting its potential in predicting the immunotherapy response in HNSCC treatment. Moreover, we found that the expression of two risk score model component genes, SETD1B and MTDH, was significantly different between tumor and the adjacent tissues in patients with LSCC, which was also significantly correlated with patient prognosis. Further experimental validation showed that the upregulated expression of MTDH significantly inhibited ferroptosis through regulating GPX4 expression and enhanced the cytotoxicity of ferroptosis inducers in HNSCC cells. In conclusion, we have developed a risk score model by using a ferroptosis-related DNA methylation signature, which can be used as an alternative tool to predict the prognosis of patients with HNSCC. SETD1B and MTDH were identified as the pivotal genes in this model and might play important role in the progression of HNSCC.

Keywords: Ferroptosis, DNA methylation, head and neck squamous cell carcinoma (HNSCC), prognosis, predictive model

Introduction

As one of the most common malignancies worldwide, head and neck squamous cell carcinoma (HNSCC) is characterized by the significantly high mortality and morbidity rate [1]. Approximately 890,000 new cases of HNSCC are diagnosed worldwide each year, along with 450,000 deaths reported by 2018 Global Cancer Report [2]. Despite the remarkable

efforts and progress over the past few decades in HNSCC management, the 5-year survival is still not significantly improved largely due to the locoregional recurrence [3, 4]. Hence, understanding the molecular mechanisms underlying the development of HNSCC to facilitate the early detection and diagnosis of HNSCC are vital to improve the prognosis and optimize the quality of life of HNSCC patients.

Programmed cell death (PCD) plays an important role in cell metabolism and tissue homeostasis [5], while the abnormal regulation of PCD is tightly linked to cancer development and progression [6, 7]. There are several forms of PCD, including apoptosis, autophagy, necrosis, pyroptosis, and ferroptosis. Among them, apoptosis is the best studied form of PCD, which is essential to maintain tissue homeostasis and to remove potentially harmful cells [8]. On the other hand, autophagy is a dynamic process that triggers self-digestion of damaged organelles and misfolded proteins in normal and tumor cells. As a result, autophagy plays a dual role in facilitating cellular adaptation to various stresses and inducing cell death during protein and organelle transformation [9, 10]. As for necrosis, it can be induced by acute injury and is characterized by cell swelling and the loss of cellular integrity [11]. Pyroptosis, a newly discovered non-apoptotic form of PCD, is closely related to the inflammatory response, which is mainly triggered by inflammatory vesicles and executed by the caspase and gasdermin protein families [12-14]. Notably, ferroptosis is a type of iron-dependent PCD discovered in 2012 and is induced by iron accumulation and lipid peroxidation [15]. Since then, many studies have demonstrated that ferroptosis-related genes are abnormally expressed in a variety of tumor types and could serve as potential therapeutic targets for cancer treatment [16, 17].

Emerging studies have indicated the regulatory role of DNA methylation, one type of epigenetic modification in gene transcription, in a variety of cellular processes [18], and the aberrant DNA methylation contributes to cancer pathogenesis [19, 20]. Especially, the hyper-methylation of tumor suppressor genes can cause epigenetic inactivation which exerts a crucial role in tumorigenesis [21]. Nonetheless, there also exists some rare DNA hypermethylation that leads to gene activation, although the underlying molecular mechanism remains unclear [22, 23]. Currently, DNA methylation information has diagnostic, predictive, and prognostic value for a diversity of cancers such as lung and breast cancers because of its stability and accuracy [24]. Importantly, accumulating evidence has suggested that DNA methylation regulates the expression of ferroptosis-related genes including GPX4 and SLC7A11 [25, 26] and that the signature constructed by ferroptosis related gene methylation may serve as a biomarker to predict the prognosis and guide the therapy options of HNSCC. In our previous study, we have investigated the interplay between m6A RNA methylation and MTDH, unraveling the potential mechanisms underlying immune therapy resistance [27]. Hence, in this study, we further delve into the pivotal role of MTDH in sensitizing ferroptosis inducers. Based on the expression of ferroptosis-associated genes, we calculated the ferroptosis score (FS) and divided HNSCC patients into the high or low FS group. Differentially methylated CpG sites (DMCs) between these two groups were further defined, and the DNA methylation related risk score was established to predict the prognosis of HNSCC patients. Moreover, we investigated the oncogenic role of MTDH and the significance of MTDH as a marker of ferroptosis inducers (**Figure 1**). Our results suggest that the DNA methylation related risk score is reliable and robust in predicting patient prognosis and providing the treatment guidance for HNSCC patients. MTDH may serve as a biomarker for the application of ferroptosis inducers.

Methods

Patients

This study retrospectively analyzed 36 cases. These patients were pathologically diagnosed with LSCC from July 2016 to August 2017 and underwent laryngectomy at the Head and Neck Nasopharyngeal Surgery Department of the Tumor Hospital of Harbin Medical University. It was reviewed and approved by the ethics committees of the two institutions and was carried out in accordance with the principles of the Declaration of Helsinki and its amendments. All participants provided informed consent to participate in the study. A total of 36 patients enrolled in the study underwent in-hospital case review and telephone follow-up until June 2022.

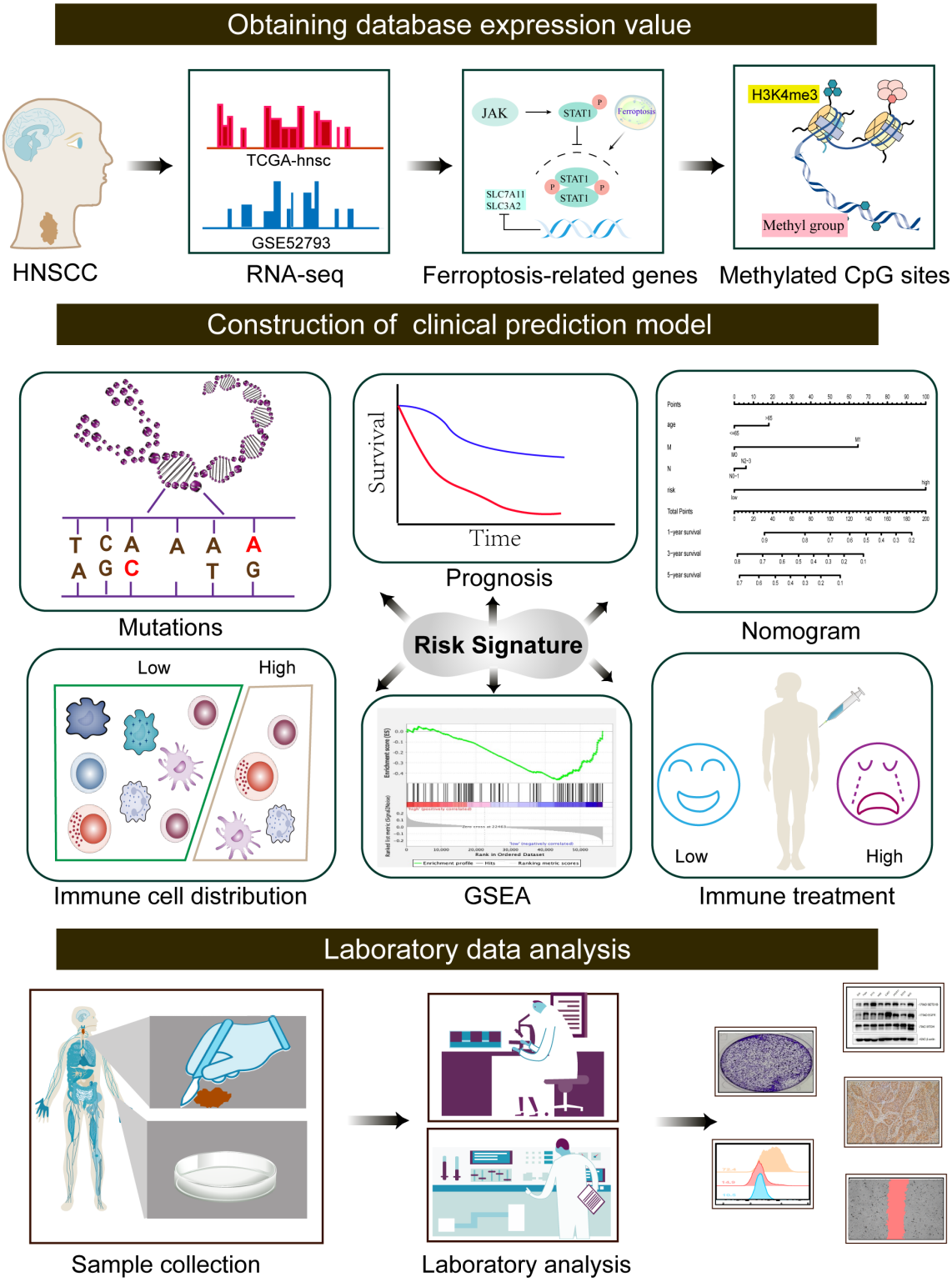

Figure 1. The flowchart of our study showing the detailed process of the research.

Clinical sample and data collection

We downloaded gene expression quantification data (FPKM and counts format) for HNSCC from TCGA (https://portal.gdc.cancer.gov/) and clinical data from the UCSC Xena website (https://xena.ucsc.edu/). Then 502 HNSCC samples and 44 normal samples were identified. We

also normalized the expression level of genes and DNA methylation level using "preprocessCore" R package. In 90% of HNSCC patients, genes whose expression was "0" were removed. From the NCBI Gene Expression Omnibus (GEO) database, an additional dataset containing methylation data of 50 OSCC patients was obtained (GSE52793).

Calculation of FS

Ferroptosis associated genes including 111 markers, 108 drivers and 69 suppressors were identified in the FerrDb database [28]. The positive and negative relationships of gene expression with overall survival in HNSCC were confirmed by univariate Cox survival analysis using the stepwise method. In the "GSVA" package, the enrichment score for genes whose expression was positively and negatively correlated with survival from HNSCC was calculated with ssGSEA [29]. Specifically, we defined 44 ferroptosis genes that were significant for univariate COX analysis as the gene set used for ssGSEA analysis. Next, we used the "ssGSEA Score" function in the "GSVA" package to calculate the ssGSEA enrichment score and adjusted it to obtain the FS score of the patient. The FS in a patient was defined as expression difference between positive and negative components which followed the method of inferring sample FS referred by Liu et al. [30]. Patients with high FS tend to show low ferroptosis activity.

Construction and evaluation based on ferroptosis-related DNA methylation signature

We determined DMCs between high and low FS group using the "limma" package and identified ferroptosis-related methylation sites associated with HNSCC survival using LASSO Cox regression analysis with the "glmnet" package. Then ferroptosis-related DNA methylation (FRDM) signature was constructed using multivariate Cox proportional hazards model. A time-dependent ROC curve analysis was performed to determine the cutoff value for FRDM signatures using the "plotROC" package [31]. The area under the ROC curve (AUC) was also identified using the "survivalROC" package. Based on the cutoff value, we divided patients into high-risk group and low-risk group. Kaplan-Meier survival curve was drawn to assess the overall survival difference between two groups using the log-rank test.

Construction and evaluation of nomograms

A nomogram was established combining the clinicopathological factors in the TCGA dataset with the FRDM signature. Using a calibration chart, we assessed the nomogram's accuracy. A decision curve analysis was then performed to compare FRSM signature risk score with clinicopathological characteristics.

Estimation of immune infiltration

The absolute abundance scores of 8 immune cells and 2 stromal cells were assessed using the "microenvironment cell population count (MCP-counter)" method [32]. A comparison of samples using the MCP-counter algorithm shows good results when assessing immune cell infiltration [33]. CIBERSORT was utilized to estimate the relative proportion of 22 infiltrating immune cells in each supplement sample. In addition, we examined the relationship between FRSM signature and molecules related to immunotherapy response using the "ggstatsplot" package.

Gene set enrichment analysis

Gene set enrichment analysis was conducted between high and low risk groups using GSEA software (version 4.0.1). The significantly enriched subset of KEGG canonical pathways and HALLMARK gene sets were identified based on GSEA.

Cell culture

Precancerous cells of human oral mucosa (Dok) and a collection of head and neck squamous carcinoma cells (Tca8113, HN8, and Cal27) were purchased from the Cell Bank of the Chinese Academy of Science (Shanghai, China). Squamous cell carcinoma of the human larynx (JHU011) came from Johns Hopkins Head and Neck Cancer Research Center (Baltimore, Maryland, USA). Other head and neck squamous cell carcinoma cell lines (FaDu, SCC4, and SAS) came from (Rockefeller, Maryland, USA). HEK293T was purchased from ATCC (CRL-3216). Cells were cultured in the DMEM (FaDu, HN8, Cal27 and HEK293T), RPMI 1640 (Dok, Tca8113, and JHU011 cells), or DMEM/F12 medium (Tu686 and SAS) (Gibco, USA) supplemented with 10% fetal bovine serum (Gibco and Inner Mongolia Opcel Biotechnology Co., Ltd.), penicillin G (100 U/ml,

Beyotime, China), streptomycin (100 μg/ml, Corning, China) in a humidifed incubator with 5% CO_2, at 37°C. All cell lines were tested and confirmed to be free of mycoplasma.

Western blotting analysis

Whole-cell protein extracted from those cells were lysed with a RIPA bufer (Beyotime, Wuhan, China) containing protease inhibitor mix (GE Healthcare, Piscataway, USA) and phosphatase inhibitor cocktail (Termo, Rockford, IL, USA). And proteins were quantifed using a BCA protein assay kit (Beyotime, Wuhan, China) according to the manufacturer's instructions. Equal amounts of cell lysate were electrophoresed in SDS-PAGE (10%) and transferred to PVDF membranes. After blocking with 5% skimmed milk in TBST at room temperature for 1 h, the membranes were incubated overnight at 4°C with primary antibodies against SETD1B (1:1000, Proteintech, 55005-1-AP), MTDH (1:1000, Proteintech, 13860-1-AP), and β-Actin (1:1000, Cell Signaling Technology, 3700S), Vinculin (1:20000, Abcam, ab129002), FSP1 (1:2000, Abclonal, A22278), SLC7A111 (1:1000, Abcam, ab307601), DHODH (1:1000, Abcam, ab174288), GPX4 (1:2000, Abcam, ab125066). After washing with TBST, the membranes were incubated with a secondary antibody (1:3000, Cell Signaling Technology, USA) for 1 h at room temperature. Finally, an ECL detection system was used to detect targeted protein bands. β-Actin was used as internal controls for western blotting.

Immunohistochemistry

The expressions of SET Domain Containing 1B (SETD1B) and Metadherin (MTDH) on the laryngeal cancer tissue were performed by immunohistochemistry (IHC) staining. Tissue sections were incubated with a primary antibody against SETD1B (1:100, Proteintech) or MTDH (1:400, Proteintech) at 4°C overnight and then incubated with reaction booster fluid at room temperature for 20 min, horseradish peroxidase combined with goat anti-mouse/rabbit antibody (PV-9000, ZSGB) at room temperature for 20 min. Tissue sections were stained using DAB and counterstained with hematoxylin. The results of the experiment were analyzed by two doctors and two pathologists. The rules are as follows: 7, about 50% of tumor cells are strongly stained; 6, about 50% of tumor cells are weakly stained; 5, about 25% of tumor cells are strongly stained; and 4, about 25% of tumor cells showed weak staining; 3, 5-25% of tumor cells showed strong staining; 2, about 5-25% of tumor cells showed weak staining; 1, < 1% of tumor cells showed low or no staining; 0, no staining was detected in the tumor cells (0%). Samples with a staining score of 0-2 were considered low expression, while samples with a score of 3-7 were considered high expression.

Lentiviral-mediated sgRNA transduction

HNSCC cell lines Fadu and HN8 were either transfected with LentiCRISPR-sgNC and LentiCRISPR-sgMTDH using viral transduction using lentiviral particles of LentiCRISPR-sgNC and LentiCRISPR-sgMTDH produced in HEK-293T cells by FuGENE 6 Tranfection Reagent (Promega) and lentiviral packaging plasmid psPAX2 (Addgene, 12260) and VSV-G envelope expressing plasmid pMD2.G (Addgene, 12259). Stable cell lines were established post-puromycin selection and were subject to cellular assays and western blot analysis. The sequence targeting MTDH is: 5'-AGAAGCCCA-AACCAAATGGG-3' and 5'-TGCGGTTGTAAGTT-GCTCGG-3'. All sgRNAs were purchased from Tsingke. All constructs were confirmed by sequencing.

Cell viability assay

Cells were seeded in 96-well plates and treated with the drugs at the appropriate time the next day. The medium with the drugs was then removed and replaced with fresh serum-free medium containing 10% Cell Counting Kit-8 (CCK8) reagent (Beyotime Biotechnology, C0038) for each well of the plate. After incubation for two hours at 37 degrees, the plates was analyzed using an ELISA reader (Biotek Synergy H4) and the absorbance of the plates was measured. Absorbance at 450 nm is proportional to the number of living cells in the culture. The reagents used in this assay, RSL3 (S8155), Erastin (S7242), Ferrostatin-1 (Fer-1) (S7243), Z-VAD-FMK (S7023) and 3-MA (S2767) were obtained from Selleck.

Lipid peroxidation assay

Lipid ROS level was analyzed by flow cytometry using BODIPY-C11 dye. Cells were seeded at a density of 20%-30% density in six-well plates and grown overnight. Cells were treated with the drugs for 12 h. The culture medium was

replaced with 2 ml medium containing 5 μM of BODIPY 581/591 C11 (Thermo Fisher, D3861), and cells were returned to the cell culture incubator for 20 min. The cells were then washed twice with 1 mL 1× PBS, digested with trypsin to obtain cell pellets, and suspended with 500 μL PBS. The cell suspension was subjected to the flow cytometry analysis to examine the amount of lipid ROS within cells. Oxidation of BODIPY-C11 resulted in a shift of the fluorescence emission peak from 590 nm to 510 nm proportional to lipid ROS generation. The fluorescence intensities of cells per sample were determined by flow cytometry using the BD FACS Aria cytometer (BD Biosciences). A minimum of 10,000 cells was analyzed per condition.

Statistical analysis

R (version 4.0.3) was used for all statistical analyses conducted in this study. $P < 0.05$ is considered as statistical significance.

Results

FS calculation based on the transcriptome data of HNSCC patients

Ferroptosis-associated genes were screened from the FerrDb database to evaluate the ferroptosis activity in HNSCC. The differential expression of ferroptosis related genes between normal and tumor tissues was presented in **Figure 2A**. Forest map showed that 44 ferroptosis related genes were identified by Cox proportional hazard regression using the stepwise method, among which 22 genes were positively or negatively correlated with survival (**Figure 2B**). Through ssGSEA analysis based on the above two gene sets, we determined the FSs of HNSCC patients as an indicator of ferroptosis activity. Then, HNSCC patients were divided into two groups according to the median FS, and the Kaplan-Meier (K-M) survival analysis was performed in the high and low FS groups. The K-M survival curve showed that patients in the high FS group had a longer overall survival (OS) compared with those in the low FS group (**Figure 2C**).

Construction of ferroptosis-related DNA methylation signature

A total of 20,381 DMCs between HNSCC patients and normal controls were identified when $P < 0.01$ and methylation difference > 0.2. We further identified 1248 DMCs between the high and low FS groups when adjusted methylation difference > 0.1 and $P < 0.01$. Finally, 378 DMCs were identified between HNSCC patients and normal controls or between the high and low FS groups, which were incorporated into the LASSO Cox regression model to screen the DMC that were strongly correlated with HNSCC survival to construct ferroptosis-related DNA methylation signature. Then, 16 CpGs with a coefficient value of not 0 were chosen and integrated into multivariate Cox model. Finally, an FRDM signature was established according to the coefficient value and the methylation level of each CpG site in multivariate Cox model. Furthermore, we explored the impact of CpG sites on the survival of HNSCC patients. The K-M curves for HNSCC patients with either a high or a low percentage of DNA methylation were presented in Figure S1A-I.

Assessment of risk model for predicting the survival of HNSCC patients

To better evaluate the predictive performance of the FRDM risk score model, we calculated the risk score for each HNSCC patient and then divided the patients into the high and low risk groups based on the median score (**Figure 3F**). We found that the risk score model was an independent risk factor for the prognosis of HNSCC patients. The AUC value of risk score and the clinicopathological factors was depicted in **Figure 3A**, showing the superior predictivity of this risk score model, while **Figure 3B** demonstrated the ROC curve of the risk score with the cut off value of 1.640. We further performed univariate and multivariate Cox proportional analyses to explore the relationship of the risk score model with other clinical factors and found that tumor metastasis and risk score were independent factors for HNSCC prognosis (**Figure 3C** and **3D**). Moreover, a K-M survival analysis revealed that patients in the high risk group had poor survival compared with those in the low risk group (**Figure 3E**), and the distribution of death increased with the increase of risk score (**Figure 3G**).

Construction and evaluation of nomograms

To improve the degree of predictive accuracy, we incorporated the risk score with other clini-

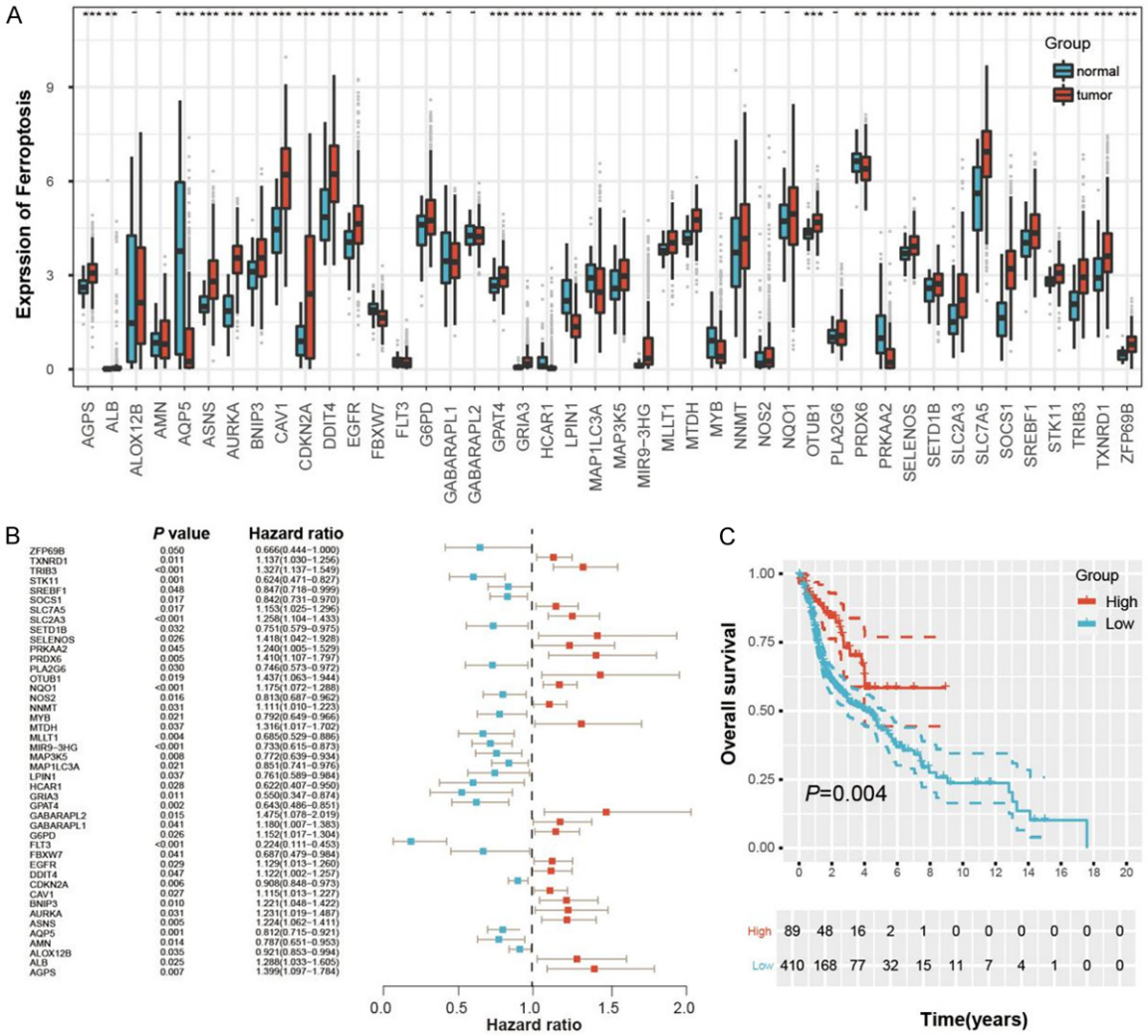

Figure 2. Correlations between FS and HNSCC overall survival. A. The expression of ferroptosis related genes between normal and tumor tissues. B. Forest map showing 44 ferroptosis related genes identified by Cox proportional hazard regression using the stepwise method. C. Kaplan-Meier survival curve of HNSCC with high and low FS group.

cal characteristics and constructed a new nomogram prediction map based on multivariate Cox proportional analysis (Figure S2A). This nomogram can be easily employed to determine the probability of 1-, 3-, and 5 year- OS by calculating the total score for each patient. The prediction calibration curve showed that four calibration points in 1, 3, 5 and 10 years were close to the standard curve, indicating the accurate predictivity of our risk score model (Figure S2B). DCA was also applied to assess the reliability of the model and showed that the risk score model curve was dramatically higher than the limit curve and clinical characteristics (Figure S2C). Importantly, we validated the predictive ability of the risk score model in a separate cohort, GSE52793. As shown in the K-M survival curve, patients with a high risk score had a shorter OS than those with a low risk score (Figure S2D). Consistently, the AUC value of the risk score model for 1-5 years' OS in GSE52793 cohort was significantly high, confirming the accurate predictive power of this model (Figure S2E and S2F).

The correlation between immune cell infiltration and the risk score model

CIBERSORT algorithm was applied to further calculate the relative proportion of 22 infiltrating immune cells in each sample. As shown in **Figure 4A**, there was a significant difference in

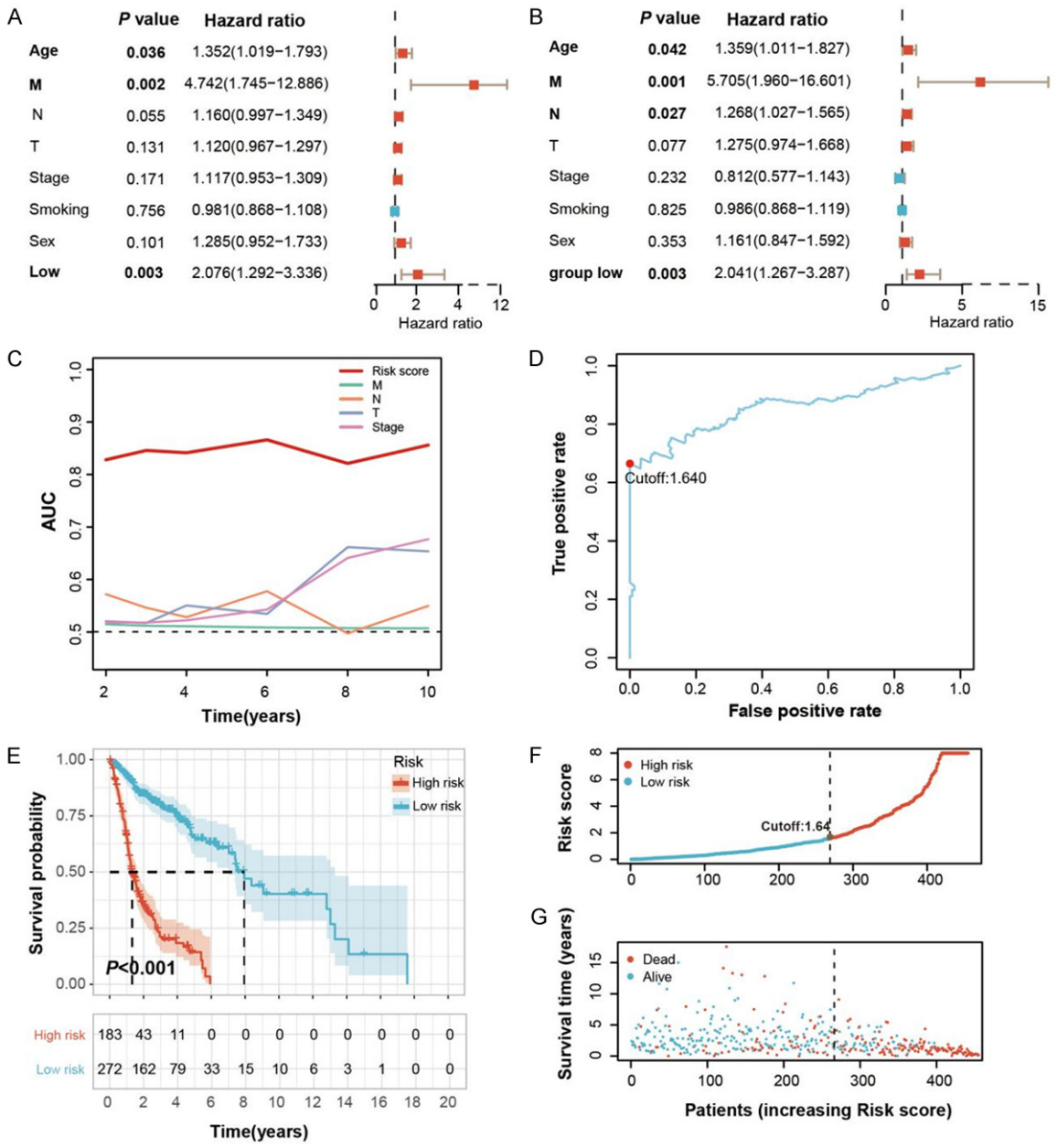

Figure 3. Correlations between ferroptosis-related DNA methylation signature and HNSCC overall survival in TCGA cohort. A. The AUC value of risk score and clinicopathological factors. B. The ROC curve of risk score with the cut off value of 1.640. C, D. Relationship of risk score with HNSCC survival using univariate and multivariate Cox proportional hazards model. E. Kaplan-Meier survival curve of HNSCC with high and low risk group. F, G. Risk score distribution and survival status in high and low risk group.

the relative proportions of CD8 T cells, CD4 memory activated T cells, Tregs, naïve B cells, and plasma cells between the high and low risk groups. We also used the MCP counter method to investigate the abundance of 8 types of immune cells as well as 2 types of stromal cells (**Figure 4C**) and found that patients with a low risk score had a higher infiltration level of B cells, CD8 T cells, dendritic cells, and T cells than those with a high risk score. In addition, the correlation between the infiltration level of immune related cells and the risk score was investigated (**Figure 4D**), and the results suggested that the immune infiltration level was negatively associated with the risk score. We further compared the survival of HNSCC

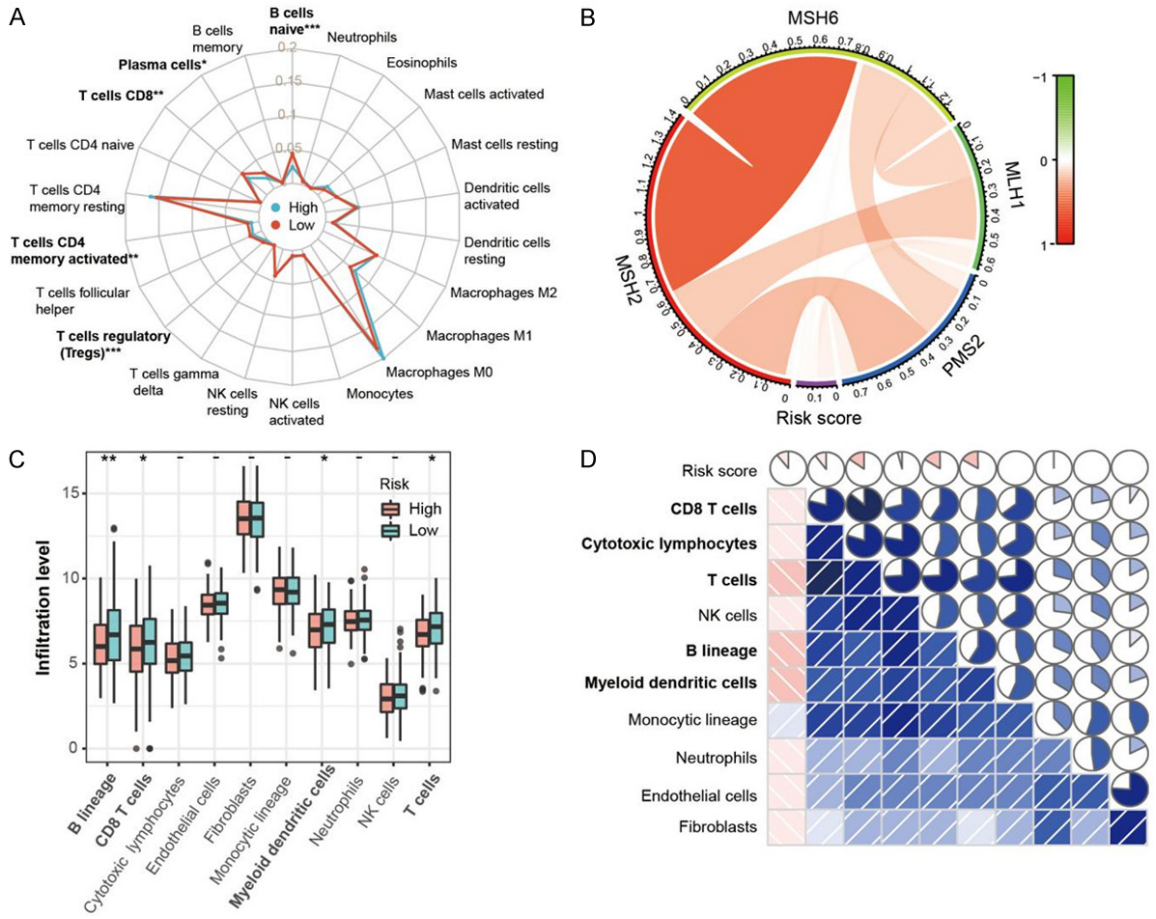

Figure 4. Correlation between risk score and immune cell infiltration. A. Radar chart of the relationship between 22 immune cell infiltration and high and low risk group. B. The relationship of mismatch repair protein including MSH2, MSH6, MLH1 and PMS2 with high and low risk group. C. The infiltration level of 8 immune cells and 2 stromal cells populations in high and low risk group using Wilcoxon rank-sum test. D. The relationship between infiltration level of immune cells and stromal cells and risk score using spearman's correlation. Area of the fan represents the degree of correlation in which a positive correlation is represented by red and a negative correlation is represented by blue.

patients between the high and low percentage of various immune cell types, as shown in Figure S3A-E. Since it has been reported that the deficiency of mismatch repair system can help detect patients who are more likely to respond to immunotherapy [34], we also explored the relationship between the risk score and the mismatch repair proteins including MSH2, MSH6, MLH1 and PMS2 (**Figure 4B**). Although no statistical significance was detected, there was a trend of a positive correlation between mismatch repair protein and the risk score.

Assessment of response to immunotherapy in the high and low risk groups

As the application of immune checkpoint inhibitors (ICIs) has dramatically changed the landscape of HNSCC treatment [35], we assessed the relationship of the risk score with immunotherapy and immune checkpoints expression in the high and low risk groups (**Figure 5A**). Compared to the low risk group, the expression of PDCD1LG2 was significantly higher in the high risk group (P=0.0081), suggesting a better clinical outcome with ICIs in the high risk population. In addition, HNSCC patients with a high risk score tend to express higher levels of CD274 and PDCD1LG2 while lower levels of PDCD1, CTLA4, LAG3, and HAVCR2 than those with a low risk score (**Figure 5B**). Furthermore, the expression of HLA-F, HLA-B, HLA-H, HLA-A, HLA-J, HLA-C and HLA-E was significantly downregulated in the low risk group (**Figure 5C**). Since immune escape is a hallmark of cancer which could be facilitated by the loss of human leukocyte antigen (HLA) [36], we speculated

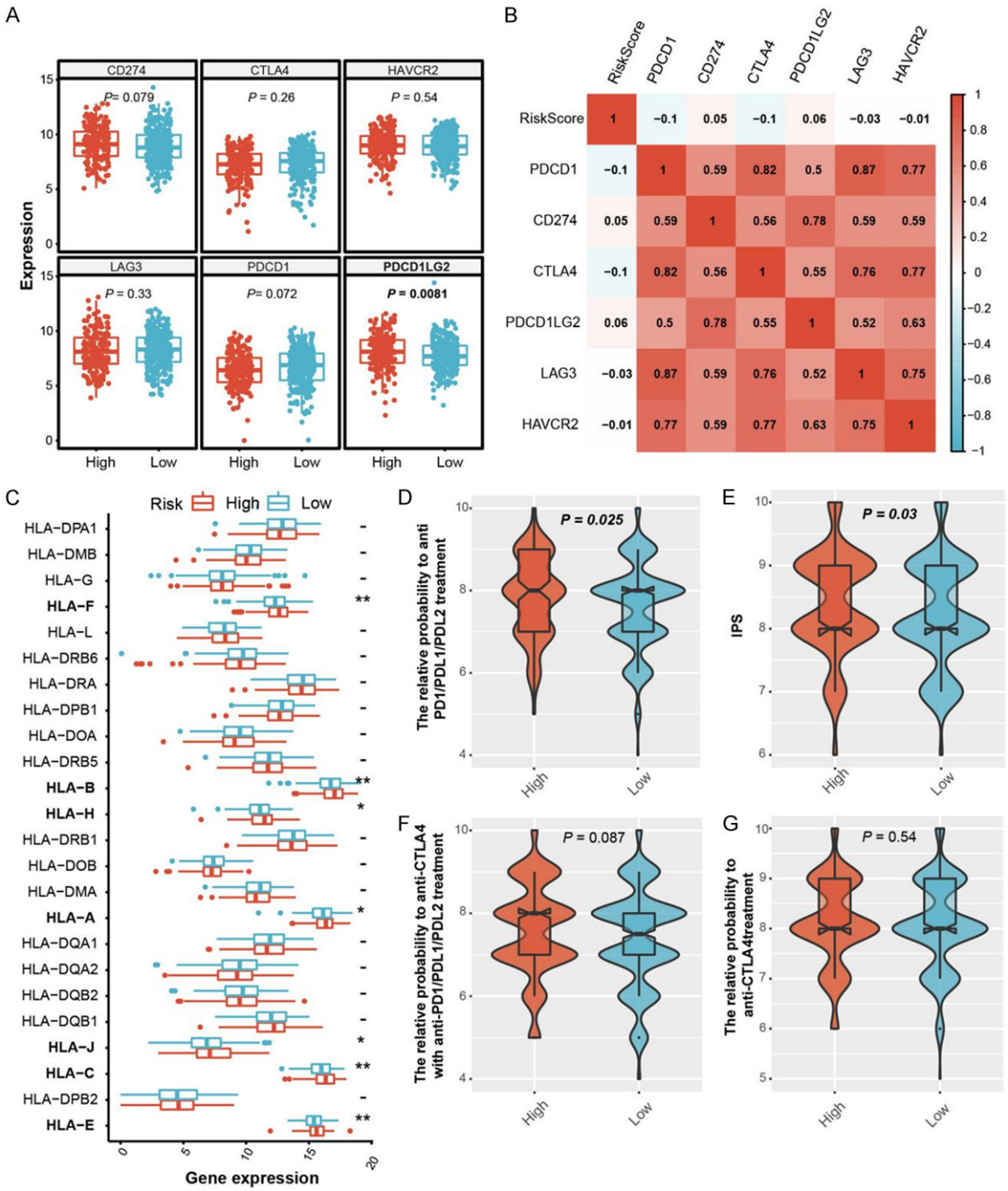

Figure 5. The relationship between risk score and immunotherapy. A. The expression of immune checkpoints in high and low risk group. B. The relationship between immune checkpoints expression and risk score using spearman's correlation. A positive correlation is represented by red and a negative correlation is represented by blue. C. The expression of HLA molecules in high and low risk group. D-G. The relative probability to immune checkpoint inhibitors and IPS difference between high and low risk group.

that patients in the low risk group will exhibit immune evasion and ICIs insensitivity. To support this, we analyzed the K-M survival curve for HNSCC patients with high and low levels of immune checkpoints, mismatch repair protein, and HLA molecules (Figure S4). As presented by violin plot in **Figure 5D**, **5F** and **5G**, the relative response probability to ICIs was higher in the high risk group, suggesting that patients in this group was more likely to benefit from ICIs

therapy. Consistently, IPS score, a quantification tool for immune checkpoint expression [37], was significantly upregulated in the high risk group (**Figure 5E**). Moreover, since tumor mutation burden (TMB) can be regarded as a strong predictive indicator for anti-tumor immune response [38], we calculated TMB and detected a significant difference between the high and low risk groups (Figure S3F).

Drug sensitivity and gene set enrichment analysis

To guide the clinical treatment of HNSCC, we compared the IC50 value of chemotherapy drugs between the high and low risk groups and found that patients in the high risk group might benefit from Vinblastine, Cetuximab, Gemcitabine, Doxorubicin treatment, while patients in the low risk group might benefit from Paclitaxel, Rapamycin and Bleomycin therapy (Figures S5A-H, S6). Sine our risk score model was tightly related to the survival, immune infiltration and ICIs efficacy in HNSCC patients, we conducted functional enrichment analysis to reveal the signaling pathways associated with risk score. The results showed that the high risk group was significantly enriched in proteasome, NOD like receptor signaling pathway, and ECM receptor interaction pathway, while the low risk group was enriched in primary immunodeficiency and intestinal immune network for IgA production (Figure S5I). Additionally, GSEA was also performed to identify the biological processes related with the risk score model. Seven hallmarks, including INTERFERON_ALPHA_RESPONSE, ANGIONENESIS, EPITHELIAL_MESENCHYMAL_TRANSITION, INTERFERON_GAMMA_RESPONSE, HYPOXIA and APOPTOSIS were correlated with high risk scores, indicating that these biological processes may contribute to HNSCC progression. In contrast, one hallmark, KRAS_SIGNALING_ON, was correlated with low risk scores, suggesting that it may improve the survival of HNSCC patients as a protective factor (Figure S5J).

Experimental validation of the risk score model

Since SETD1B and MTDH have been reported to be related to iron-induced death and are differentially expressed in our analysis, they were selected for further experimental validation. First, the protein levels of SETD1B and MTDH in HNSCC cell lines and immortalized epithelial cells DOK were examined by western blot, and the results showed that the protein level of SETD1B in HNSCC was upregulated in HNSCC cells, especially in Tca8113 and JHU011 cells, while the expression of MTDH was significantly higher in SAS and SCC4 cells than in DOK cells (**Figure 6A**). In addition, we performed immunohistochemical staining of SETD1B and MTDH in tumor and adjacent normal samples obtained from 36 HNSCC patients who were enrolled in the study. Consistently, both SETD1B and MTDH expression levels were significantly higher in tumor samples than in adjacent normal samples (**Figure 6B**, **6C**). By further integrating patient survival information, we found that the patients' survival time was prolonged with the increased SETD1B expression level (P=0.045). However, the survival time of patients was gradually decreased with the increased MTDH expression (P=0.019), which was consistent with the online database sample information (**Figure 6D**, **6E**).

Inhibiting MTDH expression reduced the proliferation and ferroptosis of HNSCC cells

To directly investigate the effect of MTDH on the phenotype of HNSCC cells, we knocked down the expression level of MTDH in Fadu and HN8 cells, which was confirmed by western blot analysis. Notably, the depletion of MTDH markedly elevated the expression level of GPX4, while the effect on other ferroptosis-related proteins was less pronounced (**Figure 7A**). In addition, the knockdown of MTDH resulted in a substantial reduction in both the colony formation and the migration of Fadu and HN8 cells (**Figure 7B-F**). Furthermore, since MTDH depletion affected the expression level of GPX4, we explored the effect of MTDH depletion on type I and type II ferroptosis inducers-induced cell death. Compared to the control group, the MTDH knockdown group exhibited more tumor cell survival. Further cell proliferation examination by using CCK-8 assay revealed that the knockdown of MTDH significantly suppressed the RSL3- and erastin-induced cell death in HNSCC cells (**Figure 8A-D**). However, this effect was abrogated by ferroptosis inhibitor ferrostatin-1, but not by apoptosis inhibitor Z-VAD-FMK and autophagy inhibitor 3-MA (**Figure 8E-H**), indicating a ferroptosis-mediated cell

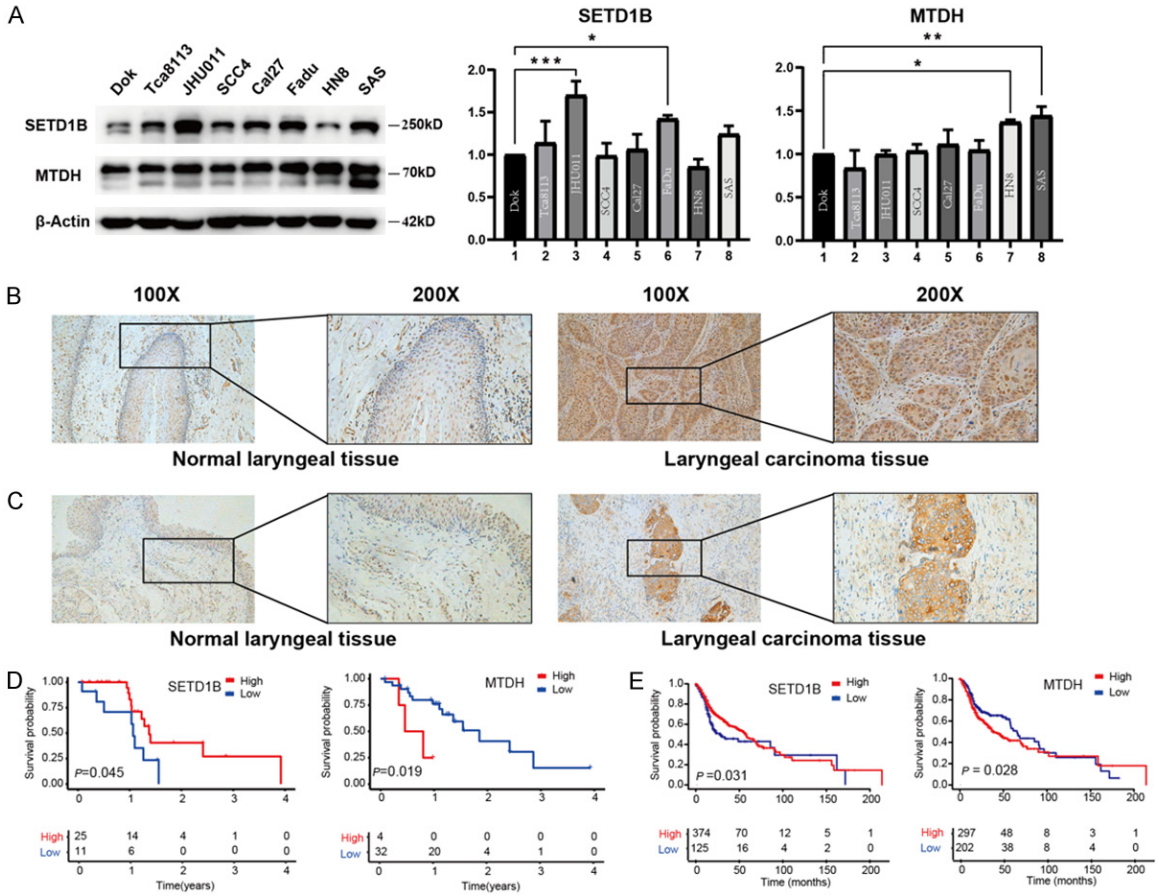

Figure 6. SETD1B and MTDH gene expression levels were associated with clinical outcomes. A. WB was used to detect the expression of SETD1B and MTDH protein in DOK of immortalized epithelial cells and HNSCC cell lines. B, C. We selected 4 representative immunohistochemical pictures to show the expression of SETD1B and MTDH in tissues. D. The Kaplan-Meier curve showed that high SETD1B and low MTDH expression were associated with higher OS in LSCC patients, and the *p* value was calculated by log-rank test (All P < 0.05). E. Kaplan-Meier curve of OS associated with SETD1B and MTDH risk stratification in external database.

death. In consistent with this finding, the ferroptosis inducers-induced ROS level was significantly higher in MTDH depleted HNSCC cells (**Figure 8I** and **8J**).

Discussion

As a new form of cell death, ferroptosis plays an important role in cancer development and progression [39]. Not only novel therapies targeting ferroptosis provide new strategies in the treatment of cancers including HNSCC [40, 41], but also ferroptosis related genes are considered as promising biomarkers of HNSCC prognosis [42, 43]. Likewise, DNA methylation has also been widely investigated and applied in predicting the prognosis of various cancer types due to its accuracy and stability [44]. Notably, ferroptosis activity can be modulated by DNA methylation through the regulation of corresponding gene transcription [25]. Thus, the risk score model based on the methylation of ferroptosis related genes could be an efficient predictive indicator in the diagnosis and prognosis of HNSCC.

In our study, we analyzed the methylome, transcriptome and clinical data in TCGA database as well as calculated the FS for each HNSCC patient based on the expression of ferroptosis related genes that were strongly related with survival. The K-M curve was further applied to determine the relationship of FS with HNSCC prognosis. We found that patients with high FS had shorter OS than those with low FS (P < 0.05), suggesting the correlation between FS and patient survival. We further identified DMCs between the high and low FS group and

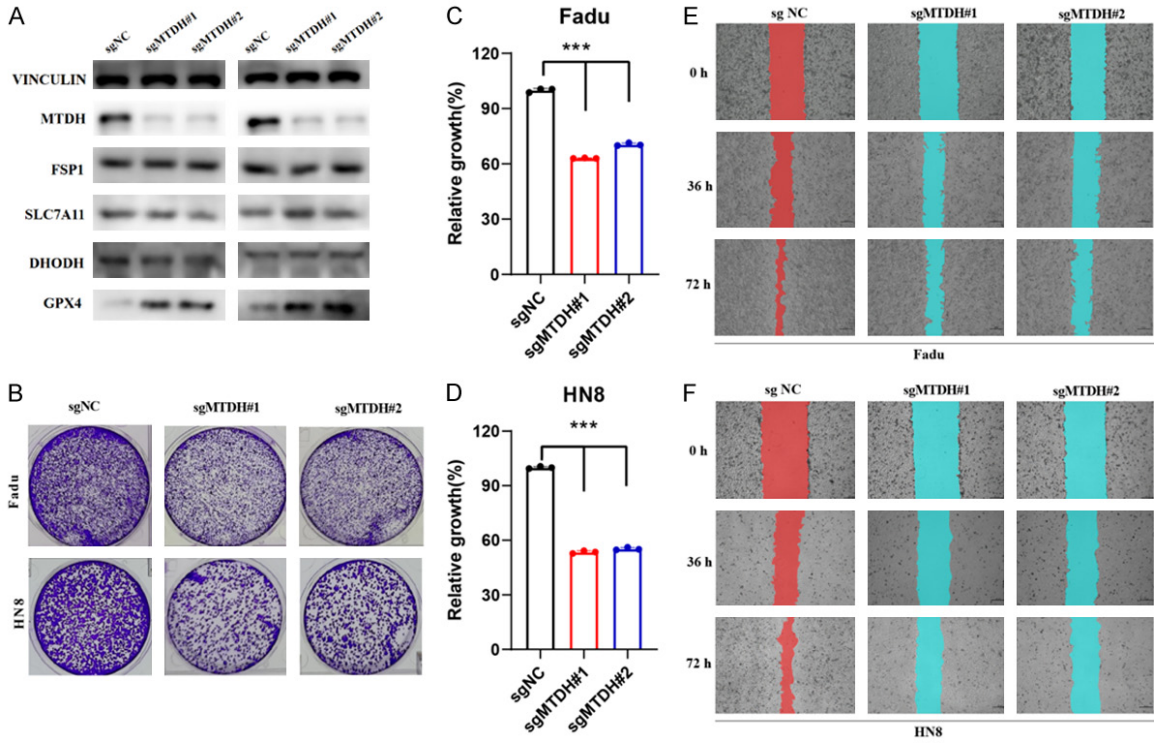

Figure 7. MTDH deletion inhibited the malignant phenotype of head and neck tumor cells and inhibited ferroptosis. (A) Levels of ferroptosis-related genes were examined in MTDH-knockdown Fadu cells or HN8 cells by western blots. Vinculin (VCL) was used as a loading control. (B) Colony formation of Fadu and HN8 cells following 10 days MTDH knockdown. Colonies were visualized by crystal purple staining. Scramble (sgNC) conditions are also displayed. (C, D) Relative Growth of MTDH-knockdown Fadu (C) or HN8 (D) cells were detected by acetic acid dissolution. (E, F) Scratch wound-healing assays (magnification, ×100) were performed to detect the effects of MTDH on the migration and invasion of MTDH-knockdown Fadu cells (E) or HN8 cells (F). Data represent mean ± SEM, n=3 independent repeats. *P* values were determined using 1-way repeated measures ANOVA (E, F).

incorporated them into the construction of risk score model. As revealed by ROC curve analysis, the AUC value of risk score model was significantly higher than that of clinical factors, which was also validated in GSE52793 cohort, indicating the superior predictive performance of our risk score model. To further optimize the predictive power of our model, a nomogram combining risk score and clinical characteristics was established, which exhibited excellent accuracy and reliability.

Moreover, we explored the difference in immune infiltration landscape between the high and low risk groups and revealed that the low risk group had higher infiltration levels of B cells, CD8 T cells, dendritic cells and T cells, whereas the high risk group was infiltrated with higher levels of macrophages and mast cells. Previous studies have indicated that the infiltration of T cells, specifically CD8+ T cells, is a good predictor of survival [45, 46]. A high level infiltration of B cells and dendritic cells is also known to have anti-tumor activity [47, 48]. In contrast, the activated mast cells are reported to play pro-tumorigenic roles in malignancies [49]. Similarly, macrophages were believed to contribute to tumor development and growth, causing aggressive phenotypes and chronic inflammation in most tumors. For example, a poor prognosis is associated with macrophage infiltration in breast cancer, bladder cancer and gastric cancer [50-52].

Immunotherapy related biomarkers such as immune checkpoints, HLA and TMB can help stratify patient subpopulations who are more likely to benefit from therapies with ICIs [53-55]. In this study, we observed that immune checkpoints including PDCD1LG2 and CD374 were highly expressed in the high risk group, whereas PDCD1, CTLA4, LAG3 and HAVCR2 were highly expressed in the low risk group, although the molecular mechanisms underly-

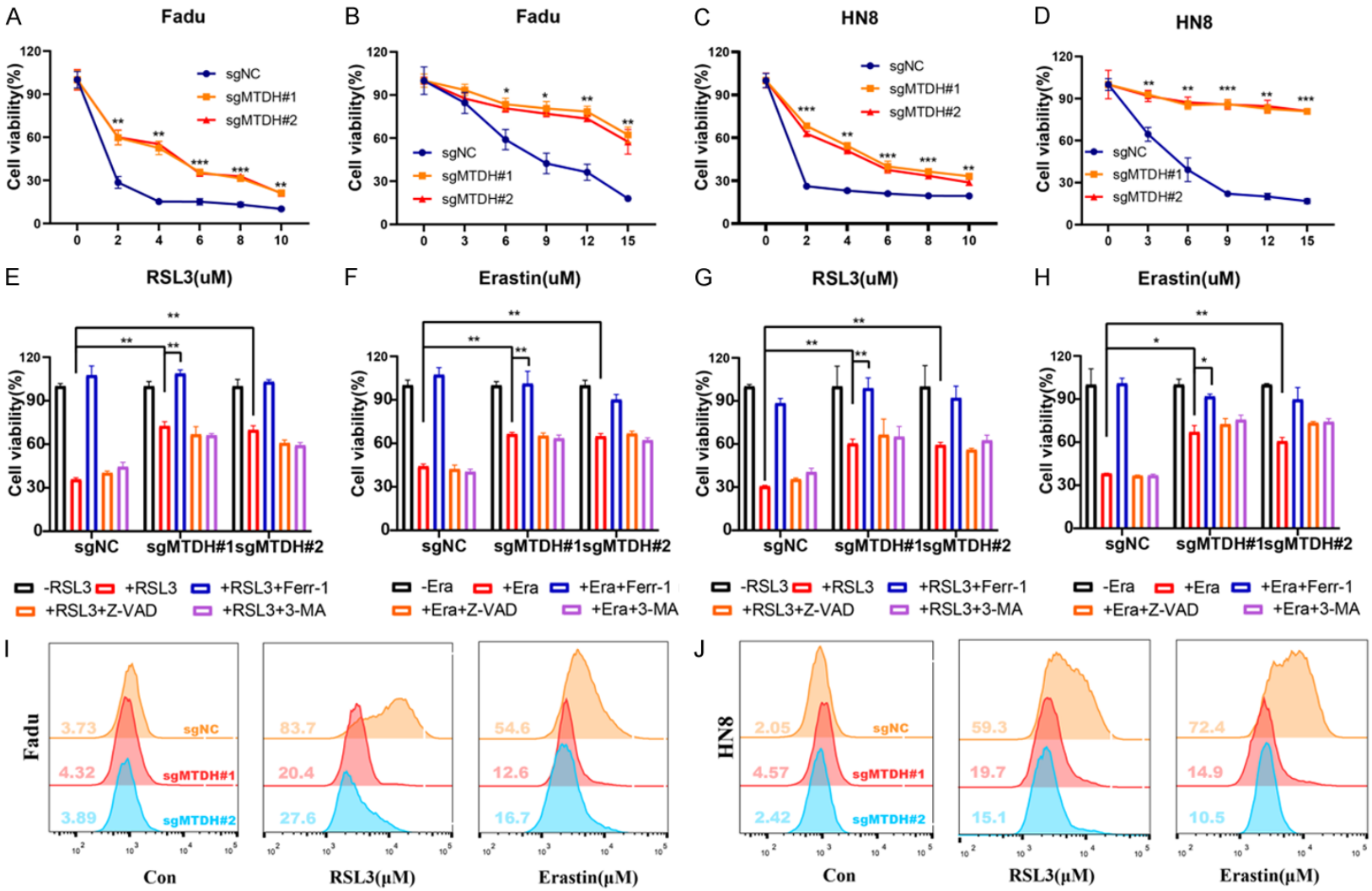

Figure 8. MTDH deletion inhibits cell death induced by ferroptosis inducers. (A-D) Knockdown of MTDH suppressed ferroptosis. MTDH-knockdown Fadu cells (A, B) or HN8 cells (C, D) was treated with different concentrations of RSL3 or Erastin for 48 h. The cells were exposed to 0.1% DMSO as control. Cell viability was assayed using a CCK8 kit. (E-H) Cell viability of MTDH-knockdown Fadu cells (E, F) or HN8 cells (G, H) was measured after treated with RSL3 (6 μm) or Erastin (9 μm) combined with Ferr-1, Z-VAD, or 3-MA for 48 h. (I, J) Lipid peroxidation was measured by flow cytometry after C11-BODIPY staining in MTDH-knockdown Fadu cells (I) or HN8 cells (J). Data represent mean ± SEM, n=3 independent repeats. *P* values were determined by 1-way repeated measures ANOVA (A-D) or 1-way ANOVA with Tukey's multiple comparison test (E-H).

ing this difference require further investigation. Additionally, our results showed that the HLA family including HLA-F, HLA-B, HLA-H, HLA-A, was downregulated in the low risk group, which might cause tumor immune evasion and immunotherapy insensitivity. It is known that tumors with a higher TMB tend to produce more new antigens and are more easily recognized by the immune system, thereby leading to better immune response. In this study, we found a higher level of TMB in HNSCC patients in the low risk group, suggesting that patients in this group may benefit more from immunotherapy.

As chemotherapy was the standard treatment for recurrent and metastatic HNSCC [56], we also investigated the ability of this risk model in predicting the efficacy of chemotherapy for HNSCC patients. By comparing the IC50 value of several chemotherapeutic agents between the low and high risk groups, we found this model could stratify subgroups that might benefit from chemotherapy, thus helping treatment decision making.

SETD1B is a ferroptosis related gene, and its frameshift mutations as well as its regional heterogeneity in gastric and colorectal cancers with high microsatellite instability were first reported by Choi et al. [57]. It is worth noting that SETD1B has been reported as an oncogene [58]; however, in this study, we found that it was highly expressed in HNSCC tumor tissues and that this high expression was associated with a better prognosis of patients. We demonstrated that SETD1B could inhibit the tumorigenesis and progression of HNSCC. Therefore, its specific functional mechanism remains to be elucidated. MTDH, one of the most common oncogenes, facilities cancer progression mainly through two mechanisms: enabling tumors to withstand the stress of chemotherapy and to escape from immune surveillance [59]. MTDH has been reported to promote the progression of a variety of tumors, including breast cancer, colorectal cancer, hepatocellular carcinoma, and glioma [60-63]. Consistent with the study by Liu et al., we found that the high expression of MTDH was significantly correlated with the poor prognosis of HNSCC patients [64]. Furthermore, the overexpression of MTDH enhanced the sensitivity of HNSCC cells to ferroptosis inducers. However, since MTDH also promotes the malignant phenotype of tumor cells, this dual role of MTDH should be considered when targeting MTDH for cancer treatment.

Although our risk score model showed excellent predictive power for the prognosis and therapy efficacy of HNSCC, there were some limitations in this study. First, our results on the efficacy of immunotherapy need to be further confirmed with HNSCC patients. Second, to apply the risk score model in clinical settings, additional clinical and functional studies are required for further validation. Lastly, the functional mechanisms by which SETD1B and MTDH impact the different clinical outcomes in patients need to be elucidated.

In conclusion, we established a risk score model based on ferroptosis-related DNA methylation signature which could serve as a potential biomarker to assess the prognosis of HNSCC patients, stratify high risk population and achieve precision therapy. In addition, we identified MTDH as a sensitizer for ferroptosis inducers, highlighting its potential as a novel therapeutic target.

Acknowledgements

We would like show sincere appreciation to the editors and reviewers for critical comments on this article. This study was supported by the Fundamental Research Funds for the Central Universities of Central South University (2023ZZTS0584).

Disclosure of conflict of interest

None.

Address correspondence to: Yong Liu and Xin Zhang, Department of Otolaryngology Head and Neck Surgery, Xiangya Hospital, Central South University, No. 87 Xiangya Road, Changsha 410008, Hunan, The People's Republic of China. E-mail: liuyongent@csu.edu.cn (YL); xinzhang@csu.edu.cn (XZ)

References

[1] Johnson DE, Burtness B, Leemans CR, Lui VWY, Bauman JE and Grandis JR. Head and neck squamous cell carcinoma. Nat Rev Dis Primers 2020; 6: 92.

[2] Bray F, Ferlay J, Soerjomataram I, Siegel RL, Torre LA and Jemal A. Global cancer statistics 2018: GLOBOCAN estimates of incidence and mortality worldwide for 36 cancers in 185

countries. CA Cancer J Clin 2018; 68: 394-424.
[3] Monnerat C, Faivre S, Temam S, Bourhis J and Raymond E. End points for new agents in induction chemotherapy for locally advanced head and neck cancers. Ann Oncol 2002; 13: 995-1006.
[4] Du E, Mazul AL, Farquhar D, Brennan P, Anantharaman D, Abedi-Ardekani B, Weissler MC, Hayes DN, Olshan AF and Zevallos JP. Long-term survival in head and neck cancer: impact of site, stage, smoking, and human papillomavirus status. Laryngoscope 2019; 129: 2506-2513.
[5] Fuchs Y and Steller H. Programmed cell death in animal development and disease. Cell 2011; 147: 742-758.
[6] Mishra AP, Salehi B, Sharifi-Rad M, Pezzani R, Kobarfard F, Sharifi-Rad J and Nigam M. Programmed cell death, from a cancer perspective: an overview. Mol Diagn Ther 2018; 22: 281-295.
[7] Chen X, Zeh HJ, Kang R, Kroemer G and Tang D. Cell death in pancreatic cancer: from pathogenesis to therapy. Nat Rev Gastroenterol Hepatol 2021; 18: 804-823.
[8] Morana O, Wood W and Gregory CD. The apoptosis paradox in cancer. Int J Mol Sci 2022; 23: 1328.
[9] Su Z, Yang Z, Xu Y, Chen Y and Yu Q. Apoptosis, autophagy, necroptosis, and cancer metastasis. Mol Cancer 2015; 14: 48.
[10] Wimmer K, Sachet M and Oehler R. Circulating biomarkers of cell death. Clin Chim Acta 2020; 500: 87-97.
[11] Zapletal E, Vasiljevic T, Busson P and Matijevic Glavan T. Dialog beyond the grave: necrosis in the tumor microenvironment and its contribution to tumor growth. Int J Mol Sci 2023; 24: 5278.
[12] Kovacs SB and Miao EA. Gasdermins: effectors of pyroptosis. Trends Cell Biol 2017; 27: 673-684.
[13] Fang Y, Tian S, Pan Y, Li W, Wang Q, Tang Y, Yu T, Wu X, Shi Y, Ma P and Shu Y. Pyroptosis: a new frontier in cancer. Biomed Pharmacother 2020; 121: 109595.
[14] Du T, Gao J, Li P, Wang Y, Qi Q, Liu X, Li J, Wang C and Du L. Pyroptosis, metabolism, and tumor immune microenvironment. Clin Transl Med 2021; 11: e492.
[15] Dixon SJ, Lemberg KM, Lamprecht MR, Skouta R, Zaitsev EM, Gleason CE, Patel DN, Bauer AJ, Cantley AM, Yang WS, Morrison B 3rd and Stockwell BR. Ferroptosis: an iron-dependent form of nonapoptotic cell death. Cell 2012; 149: 1060-1072.
[16] Jiang L, Kon N, Li T, Wang SJ, Su T, Hibshoosh H, Baer R and Gu W. Ferroptosis as a p53-mediated activity during tumour suppression. Nature 2015; 520: 57-62.
[17] Yee PP, Wei Y, Kim SY, Lu T, Chih SY, Lawson C, Tang M, Liu Z, Anderson B, Thamburaj K, Young MM, Aregawi DG, Glantz MJ, Zacharia BE, Specht CS, Wang HG and Li W. Neutrophil-induced ferroptosis promotes tumor necrosis in glioblastoma progression. Nat Commun 2020; 11: 5424.
[18] Bird A. DNA methylation patterns and epigenetic memory. Genes Dev 2002; 16: 6-21.
[19] Calmon MF, Jeschke J, Zhang W, Dhir M, Siebenkäs C, Herrera A, Tsai HC, O'Hagan HM, Pappou EP, Hooker CM, Fu T, Schuebel KE, Gabrielson E, Rahal P, Herman JG, Baylin SB and Ahuja N. Epigenetic silencing of neurofilament genes promotes an aggressive phenotype in breast cancer. Epigenetics 2015; 10: 622-632.
[20] Esteller M. Epigenetic gene silencing in cancer: the DNA hypermethylome. Hum Mol Genet 2007; 16: R50-59.
[21] Steinmann K, Sandner A, Schagdarsurengin U and Dammann RH. Frequent promoter hypermethylation of tumor-related genes in head and neck squamous cell carcinoma. Oncol Rep 2009; 22: 1519-1526.
[22] Suh DH, Kim MK, Kim HS, Chung HH and Song YS. Unfolded protein response to autophagy as a promising druggable target for anticancer therapy. Ann N Y Acad Sci 2012; 1271: 20-32.
[23] Spainhour JC, Lim HS, Yi SV and Qiu P. Correlation patterns between DNA methylation and gene expression in the cancer genome atlas. Cancer Inform 2019; 18: 1176935119828776.
[24] Costa-Pinheiro P, Montezuma D, Henrique R and Jerónimo C. Diagnostic and prognostic epigenetic biomarkers in cancer. Epigenomics 2015; 7: 1003-1015.
[25] Zhang X, Huang Z, Xie Z, Chen Y, Zheng Z, Wei X, Huang B, Shan Z, Liu J, Fan S, Chen J and Zhao F. Homocysteine induces oxidative stress and ferroptosis of nucleus pulposus via enhancing methylation of GPX4. Free Radic Biol Med 2020; 160: 552-565.
[26] Lohoff FW, Clarke TK, Kaminsky ZA, Walker RM, Bermingham ML, Jung J, Morris SW, Rosoff D, Campbell A, Barbu M, Charlet K, Adams M, Lee J, Howard DM, O'Connell EM, Whalley H, Porteous DJ, McIntosh AM and Evans KL. Epigenome-wide association study of alcohol consumption in N = 8161 individuals and relevance to alcohol use disorder pathophysiology: identification of the cystine/glutamate transporter SLC7A11 as a top target. Mol Psychiatry 2022; 27: 1754-1764.
[27] Zhang F, Huang H, Qin Y, Chen C, She L, Wang J, Huang D, Tang Q, Liu Y, Zhu G and Zhang X. MTDH associates with m6A RNA methylation

and predicts cancer response for immune checkpoint treatment. iScience 2021; 24: 103102.
[28] Zhou N and Bao J. FerrDb: a manually curated resource for regulators and markers of ferroptosis and ferroptosis-disease associations. Database (Oxford) 2020; 2020: baaa021.
[29] Hänzelmann S, Castelo R and Guinney J. GSVA: gene set variation analysis for microarray and RNA-seq data. BMC Bioinformatics 2013; 14: 7.
[30] Liu Z, Zhao Q, Zuo ZX, Yuan SQ, Yu K, Zhang Q, Zhang X, Sheng H, Ju HQ, Cheng H, Wang F, Xu RH and Liu ZX. Systematic analysis of the aberrances and functional implications of ferroptosis in cancer. iScience 2020; 23: 101302.
[31] Heagerty PJ, Lumley T and Pepe MS. Time-dependent ROC curves for censored survival data and a diagnostic marker. Biometrics 2000; 56: 337-344.
[32] Becht E, Giraldo NA, Lacroix L, Buttard B, Elarouci N, Petitprez F, Selves J, Laurent-Puig P, Sautès-Fridman C, Fridman WH and de Reyniès A. Estimating the population abundance of tissue-infiltrating immune and stromal cell populations using gene expression. Genome Biol 2016; 17: 249.
[33] Sturm G, Finotello F, Petitprez F, Zhang JD, Baumbach J, Fridman WH, List M and Aneichyk T. Comprehensive evaluation of transcriptome-based cell-type quantification methods for immuno-oncology. Bioinformatics 2019; 35: i436-i445.
[34] Olave MC and Graham RP. Mismatch repair deficiency: the what, how and why it is important. Genes Chromosomes Cancer 2022; 61: 314-321.
[35] Gao L, Zhang A, Yang F and Du W. Immunotherapeutic Strategies for Head and Neck Squamous Cell Carcinoma (HNSCC): current perspectives and future prospects. Vaccines (Basel) 2022; 10: 1272.
[36] Dyckhoff G, Herold-Mende C, Scherer S, Plinkert PK and Warta R. Human leucocyte antigens as prognostic markers in head and neck squamous cell carcinoma. Cancers (Basel) 2022; 14: 3828.
[37] Ozturk V, Yikilmaz AS, Kilicarslan A, Bakanay SM, Akinci S and Dilek İ. The triple positivity for EBV, PD-1, and PD-L1 identifies a very high risk classical hodgkin lymphoma. Clin Lymphoma Myeloma Leuk 2020; 20: e375-e381.
[38] Doig KD, Fellowes A, Scott P and Fox SB. Tumour mutational burden: an overview for pathologists. Pathology 2022; 54: 249-253.
[39] Lu B, Chen XB, Ying MD, He QJ, Cao J and Yang B. The role of ferroptosis in cancer development and treatment response. Front Pharmacol 2018; 8: 992.
[40] Liu HJ, Hu HM, Li GZ, Zhang Y, Wu F, Liu X, Wang KY, Zhang CB and Jiang T. Ferroptosis-related gene signature predicts glioma cell death and glioma patient progression. Front Cell Dev Biol 2020; 8: 538.
[41] Tang Y, Li C, Zhang YJ and Wu ZH. Ferroptosis-related long non-coding RNA signature predicts the prognosis of Head and neck squamous cell carcinoma. Int J Biol Sci 2021; 17: 702-711.
[42] Jiang W, Song Y, Zhong Z, Gao J and Meng X. Ferroptosis-related long non-coding RNA signature contributes to the prediction of prognosis outcomes in head and neck squamous cell carcinomas. Front Genet 2021; 12: 785839.
[43] Li Q, Jin Y, Shen Z, Liu H, Shen Y and Wu Z. Construction of a ferroptosis-related gene signature for head and neck squamous cell carcinoma prognosis prediction. Int J Gen Med 2021; 14: 10117-10129.
[44] Guo W, Zhu L, Yu M, Zhu R, Chen Q and Wang Q. A five-DNA methylation signature act as a novel prognostic biomarker in patients with ovarian serous cystadenocarcinoma. Clin Epigenetics 2018; 10: 142.
[45] Wuerdemann N, Pütz K, Eckel H, Jain R, Wittekindt C, Huebbers CU, Sharma SJ, Langer C, Gattenlöhner S, Büttner R, Speel EJ, Suchan M, Wagner S, Quaas A and Klussmann JP. LAG-3, TIM-3 and VISTA expression on tumor-infiltrating lymphocytes in oropharyngeal squamous cell carcinoma-potential biomarkers for targeted therapy concepts. Int J Mol Sci 2020; 22: 379.
[46] Bindea G, Mlecnik B, Tosolini M, Kirilovsky A, Waldner M, Obenauf AC, Angell H, Fredriksen T, Lafontaine L, Berger A, Bruneval P, Fridman WH, Becker C, Pagès F, Speicher MR, Trajanoski Z and Galon J. Spatiotemporal dynamics of intratumoral immune cells reveal the immune landscape in human cancer. Immunity 2013; 39: 782-795.
[47] Qin Y, Lu F, Lyu K, Chang A and Li Q. Emerging concepts regarding pro- and anti tumor properties of B cells in tumor immunity. Front Immunol 2022; 13: 881427.
[48] Wang Y, Yang H, Jia A, Wang Y, Yang Q, Dong Y, Hou Y, Cao Y, Dong L, Bi Y and Liu G. Dendritic cell Piezo1 directs the differentiation of T_H1 and T_{reg} cells in cancer. elife 2022; 11: e79957.
[49] Cui Y, Shen T, Xu F, Zhang J, Wang Y, Wu J, Bu H, Fu D, Fang B, Lv H, Wang S, Shi C, Liu B, He H, Tang H and Ge J. KCNN4 may weaken antitumor immune response via raising Tregs and diminishing resting mast cells in clear cell renal cell carcinoma. Cancer Cell Int 2022; 22: 211.
[50] Tu D, Dou J, Wang M, Zhuang H and Zhang X. M2 macrophages contribute to cell prolifera-

tion and migration of breast cancer. Cell Biol Int 2021; 45: 831-838.
[51] Sharifi L, Nowroozi MR, Amini E, Arami MK, Ayati M and Mohsenzadegan M. A review on the role of M2 macrophages in bladder cancer; pathophysiology and targeting. Int Immunopharmacol 2019; 76: 105880.
[52] Li W, Zhang X, Wu F, Zhou Y, Bao Z, Li H, Zheng P and Zhao S. Gastric cancer-derived mesenchymal stromal cells trigger M2 macrophage polarization that promotes metastasis and EMT in gastric cancer. Cell Death Dis 2019; 10: 918.
[53] Walk EE, Yohe SL, Beckman A, Schade A, Zutter MM, Pfeifer J and Berry AB; College of American Pathologists Personalized Health Care Committee. The cancer immunotherapy biomarker testing landscape. Arch Pathol Lab Med 2020; 144: 706-724.
[54] Sabbatino F, Liguori L, Polcaro G, Salvato I, Caramori G, Salzano FA, Casolaro V, Stellato C, Col JD and Pepe S. Role of human leukocyte antigen system as a predictive biomarker for checkpoint-based immunotherapy in cancer patients. Int J Mol Sci 2020; 21: 7295.
[55] Cao J, Yang X, Chen S, Wang J, Fan X, Fu S and Yang L. The predictive efficacy of tumor mutation burden in immunotherapy across multiple cancer types: a meta-analysis and bioinformatics analysis. Transl Oncol 2022; 20: 101375.
[56] Boguszewicz Ł. Predictive biomarkers for response and toxicity of induction chemotherapy in head and neck cancers. Front Oncol 2022; 12: 900903.
[57] Choi YJ, Oh HR, Choi MR, Gwak M, An CH, Chung YJ, Yoo NJ and Lee SH. Frameshift mutation of a histone methylation-related gene SETD1B and its regional heterogeneity in gastric and colorectal cancers with high microsatellite instability. Hum Pathol 2014; 45: 1674-1681.
[58] Chen D, Li T, Wang C, Lei G, Wang R, Wang Z, Yu L, Yan J, Zhang P, Wang X, Zhang S and Yang P. High-level SETD1B gene expression is associated with unfavorable prognosis in hepatocellular carcinoma. Mol Med Rep 2019; 19: 1587-1594.
[59] Chen Y, Huang S, Guo R and Chen D. Metadherin-mediated mechanisms in human malignancies. Biomark Med 2021; 15: 1769-1783.
[60] Neeli PK, Sahoo S, Karnewar S, Singuru G, Pulipaka S, Annamaneni S and Kotamraju S. DOT1L regulates MTDH-mediated angiogenesis in triple-negative breast cancer: intermediacy of NF-kappaB-HIF1alpha axis. FEBS J 2023; 290: 502-520.
[61] Sultan A, Sahar NE, Riaz SK, Qadir J, Waqar SH, Haq F, Khaliq T and Malik MFA. Metadherin (MTDH) overexpression significantly correlates with advanced tumor grade and stages among colorectal cancer patients. Mol Biol Rep 2021; 48: 7999-8007.
[62] Wan JL, Wang B, Wu ML, Li J, Gong RM, Song LN, Zhang HS, Zhu GQ, Chen SP, Cai JL, Xing XX, Wang YD, Yang Y, Cai CZ, Huang R, Liu H and Dai Z. MTDH antisense oligonucleotides reshape the immunosuppressive tumor microenvironment to sensitize hepatocellular carcinoma to immune checkpoint blockade therapy. Cancer Lett 2022; 541: 215750.
[63] Fu J, Peng J and Tu G. Knockdown MTDH inhibits glioma proliferation and migration and promotes apoptosis by downregulating MYBL2. Mediators Inflamm 2022; 2022: 1706787.
[64] Liu X, Lv Z, Zhou S, Kan S, Liu X, Jing P and Xu W. MTDH in macrophages promotes the vasculogenic mimicry via VEGFA-165/Flt-1 signaling pathway in head and neck squamous cell carcinoma. Int Immunopharmacol 2021; 96: 107776.

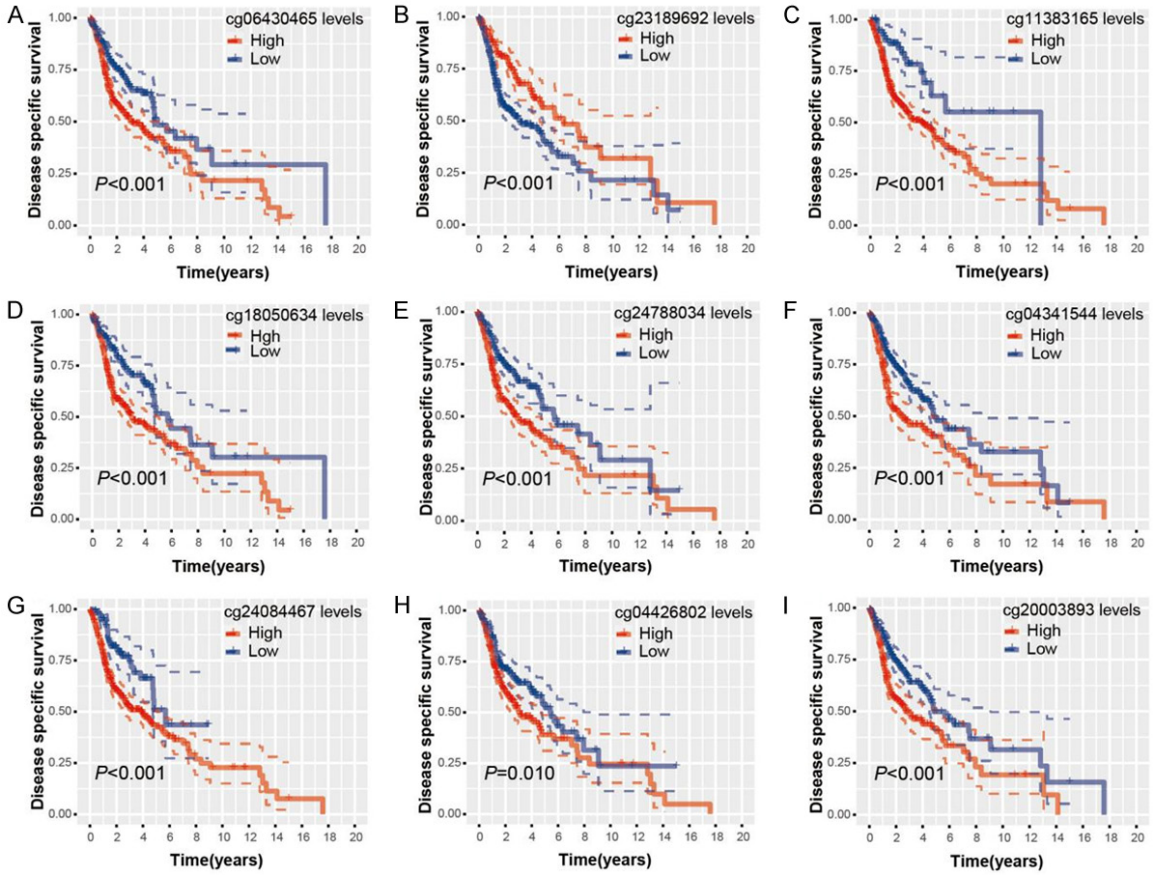

Figure S1. K-M curves for HNSCC patients with high and low percentage of DNA methylation levels.

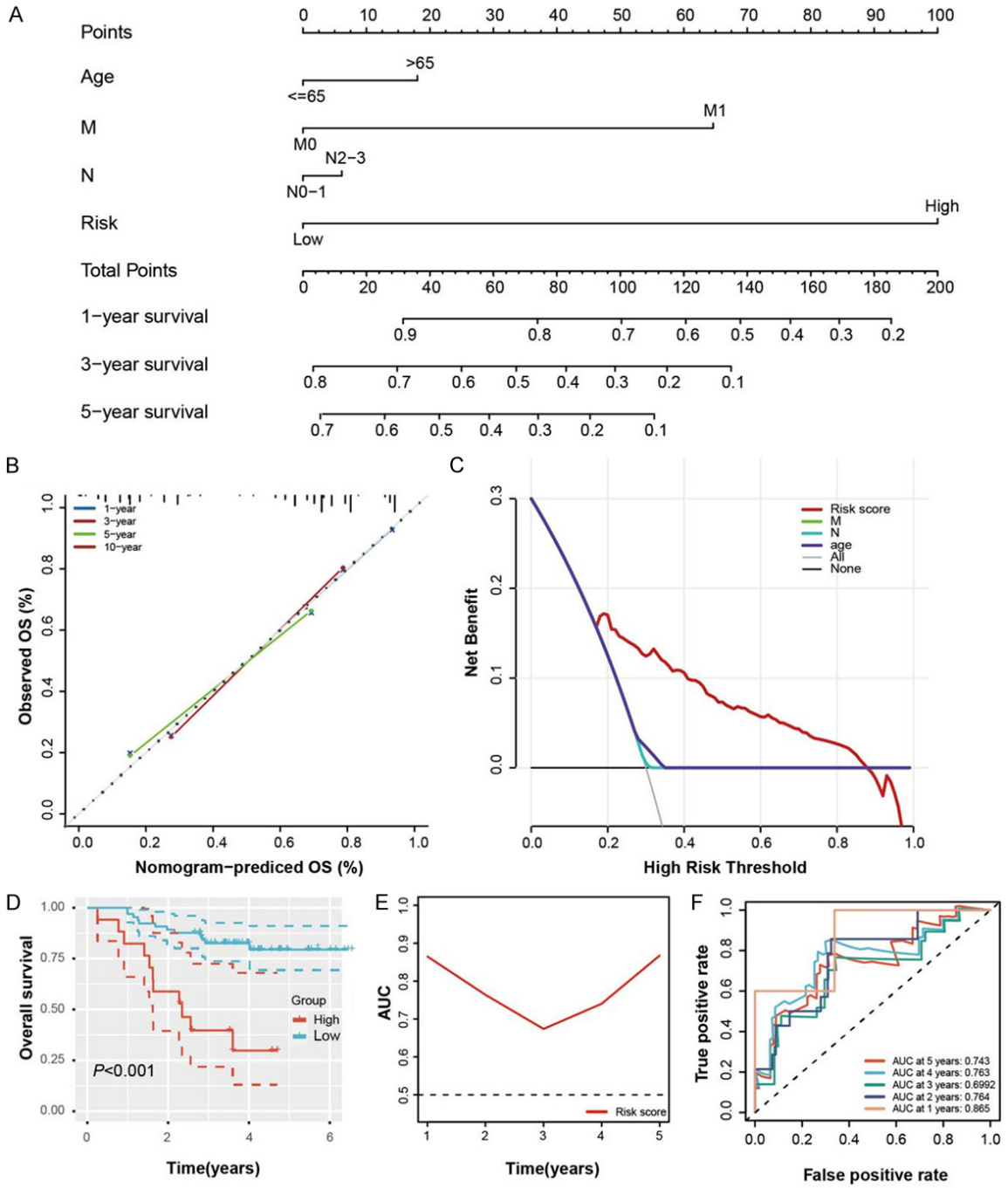

Figure S2. Construction and evaluation of clinical prognostic model. A. Nomogram predicting the probability of HNSCC patient's mortality based on risk score and clinicopathological factors. B. Calibration curves of the nomogram for 1, 3 and 5 years. C. Decision curve analysis of the nomograms based on the risk score and clinicopathological factors. D. Kaplan-Meier survival curve of HNSCC with high and low risk group in GSE52793 cohort. E. The AUC value of risk score in GSE52793 cohort. F. The ROC curve of risk score at 1-5 years in GSE52793 cohort.

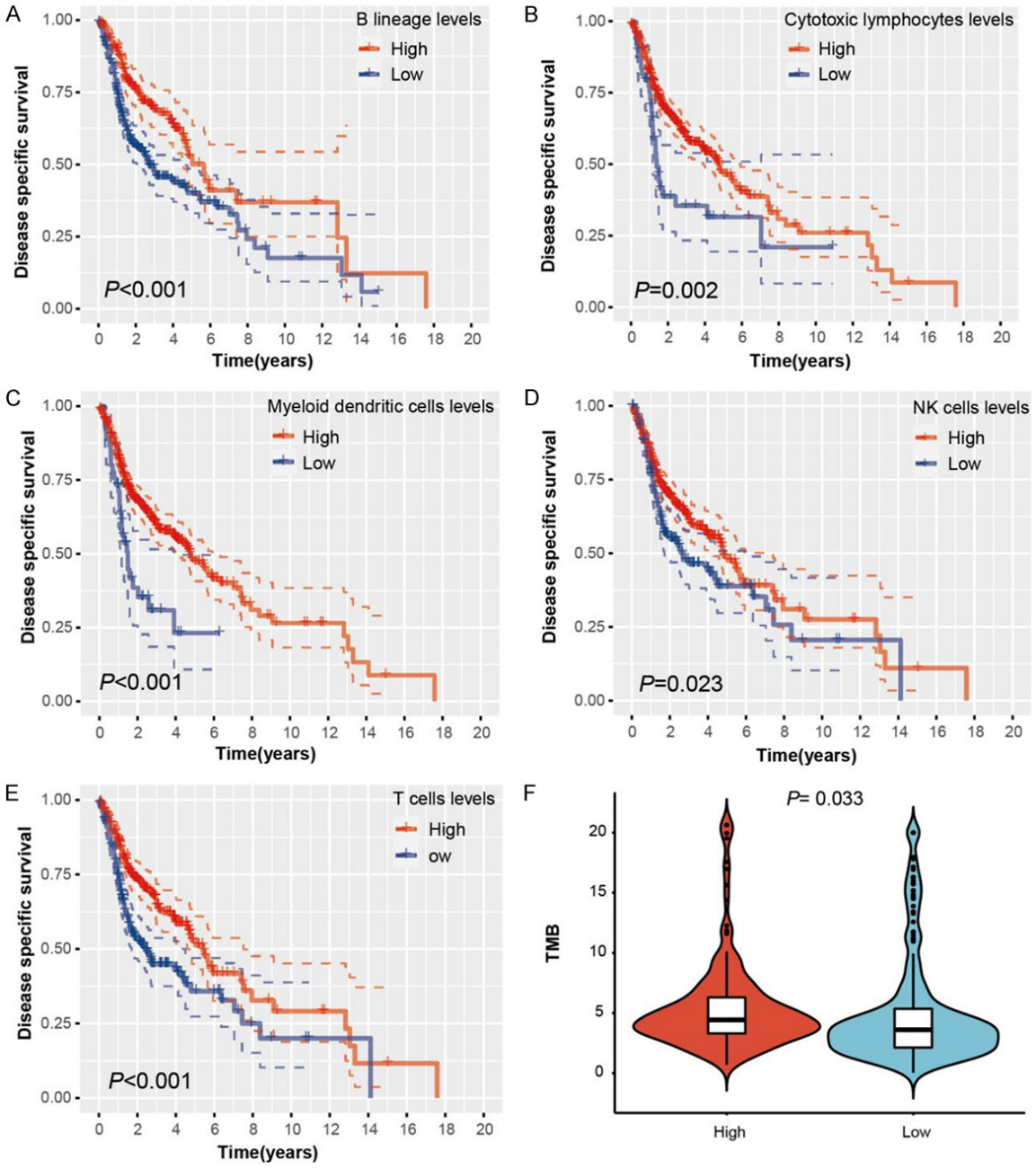

Figure S3. A-E. Kaplan-Meier survival curve for HNSCC patients with high and low percentage of various immune cell types. F. The level of TMB between high and low risk group.

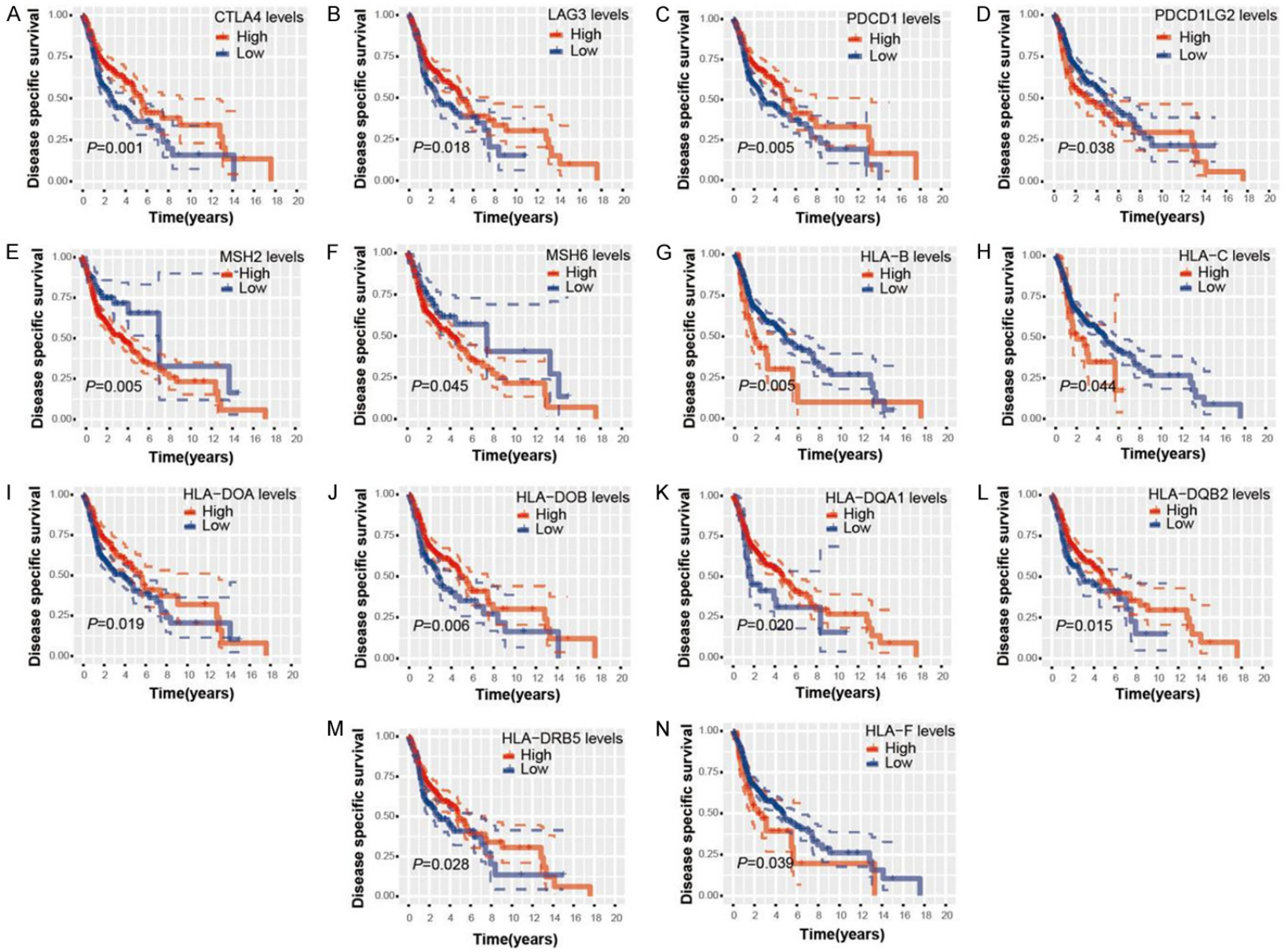

Figure S4. Kaplan-Meier survival curve for HNSCC patients with high and low percentage of immune checkpoints, mismatch repair protein and HLA molecules.

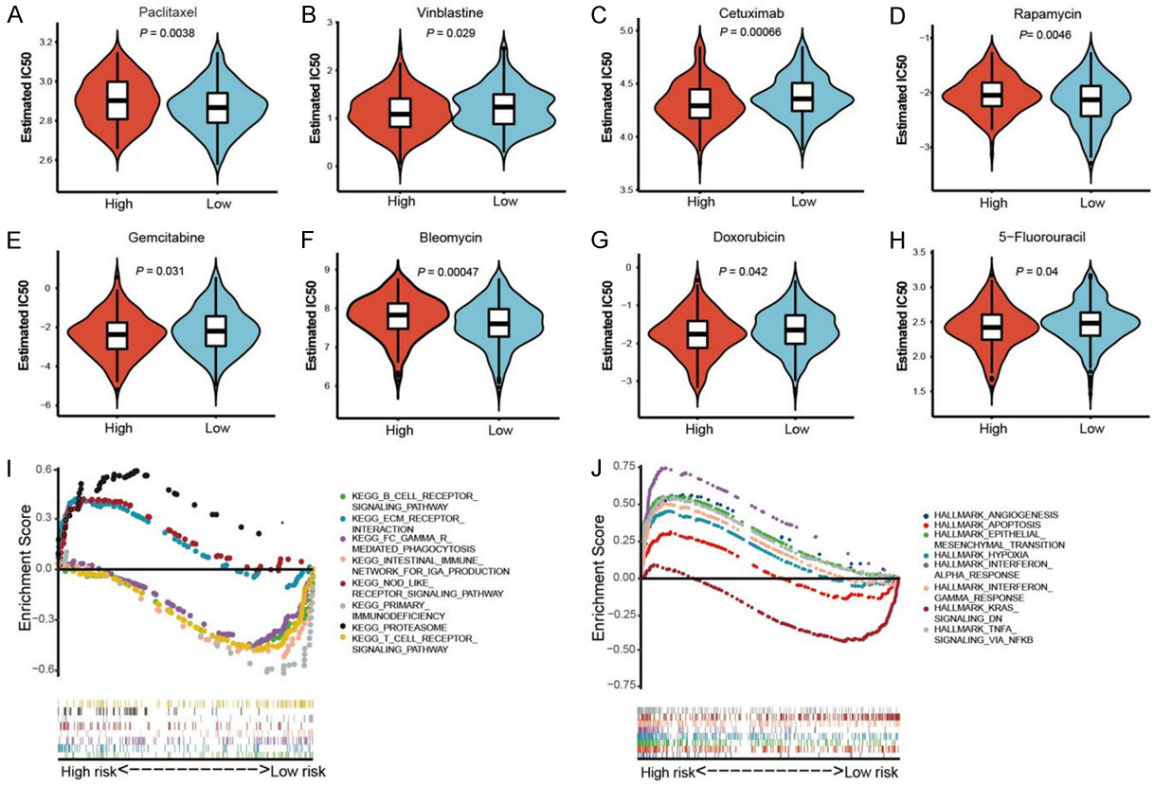

Figure S5. Drug sensitivity and gene set enrichment analysis. A-H. The estimated IC50 value of drugs between high and low risk group. I. The significantly enriched subset of KEGG canonical pathways based on GSEA. J. The significantly enriched HALLMARK gene sets based on GSEA.

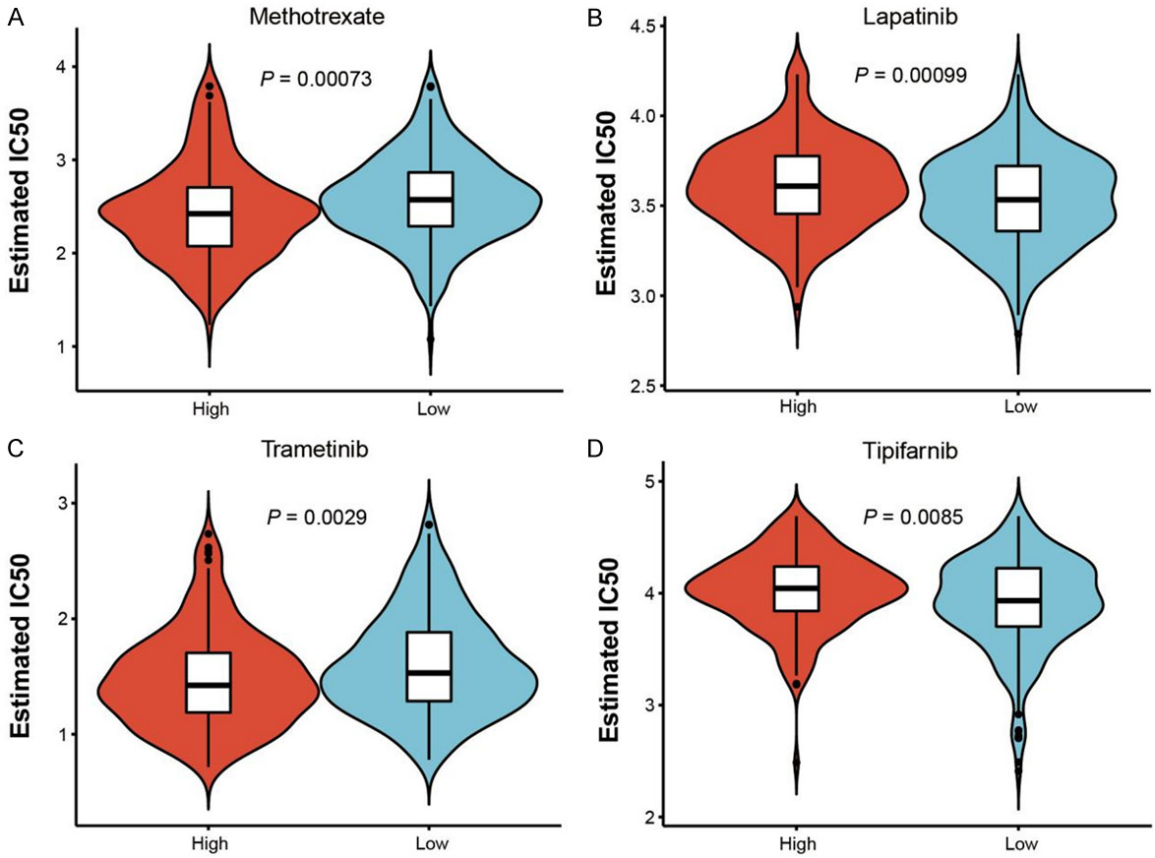

Figure S6. The estimated IC50 value of drugs between high and low risk group.